Tissue factor isoforms in cancer and blood coagulation

Kocatürk, B.

Chapter 5 - Alternatively spliced tissue factor promotes breast cancer growth in a β1 integrin-dependent manner

B Kocatürk, YW van den Berg, C Tieken , JS Mieog, EM de Kruijf, CC Engels, MA van der Ent, PJ Kuppen, CJ van de Velde, W Ruf, PH Reitsma, S Osanto, GJ Liefers, VY Bogdanov and HH Versteeg

Proc Natl Acad Sci U S A. 2013 Jul 9;110(28):11517-22.

Abstract

Full-length tissue factor (flTF), the coagulation initiator, is overexpressed in breast cancer (BrCa), but associations between flTF expression and clinical outcome remain controversial. It is currently not known whether the soluble alternatively spliced TF form (asTF) is expressed in BrCa or impacts BrCa progression. We are unique in reporting that asTF, but not flTF, strongly associates with both tumor size and grade, and induces BrCa cell proliferation by binding to β1 integrins. asTF promotes oncogenic gene expression, anchorage-independent growth and strongly up-regulates tumor expansion in a luminal BrCa model. In basal BrCa cells that constitutively express both TF isoforms, asTF blockade reduces tumor growth and proliferation *in vivo*.

We propose that asTF plays a major role in BrCa progression acting as an autocrine factor that promotes tumor progression. Targeting asTF may comprise a previously unexplored therapeutic strategy in BrCa that stems tumor growth, yet does not impair normal hemostasis.

Introduction

In breast cancer (BrCa), proteins that modulate splicing events such as ASF/SF2 and SR(Serine/Arginine-rich)p55, are frequently up-regulated and contribute to cell transformation [1, 2]. BrCa cells exhibit specific alternative splicing signatures that were proposed as potential prognostic factors in BrCa [3]. Alternative splicing of proteins such as spleen tyrosine kinase (Syk), p53, phosphatase and tensin homolog (PTEN), chemokine (C-X-C motif) receptor 3 (CXCR3) and ras-related C3 botulinum toxin substrate 1 (Rac1) impacts BrCa cell behavior and therefore, disease progression [4-8].

Full-length Tissue Factor (flTF) is the principal initiator of blood coagulation [9]. Following vascular damage, flTF binds its ligand FVII(a), which triggers clot formation. Aside from sub-endothelial tissues, flTF is also abundant on cancer cells [9] and fuels tumor progression by modulating integrin α3β1 function, cell migration [10], and fVIIa-dependent in Protease Activated Receptor (PAR)2 activation, but flTF-β1 integrin complexation enhances PAR2 activation [11]. flTF-dependent PAR2 activation results in the production of VEGF, CXCL1, and IL-8, thus promoting the angiogenic switch and consequently, tumor growth *in vivo* [10, 11] .

Alternative splicing of TF pre-mRNA results in the deletion of exon 5 and thus a frameshift in exon 6, yielding a transmembrane domain-lacking isoform that can be secreted [12].

Human and murine alternatively spliced TF (asTF) contain novel C-termini with poor homology to one another or any other protein, and the murine asTF C terminus is longer than that of human asTF [12, 13]. High expression of asTF in tumor cell lines suggests a role in tumor progression [10, 14]. Subcutaneous growth of pancreatic cancer cells overexpressing asTF, results in larger and more vascularized tumors [15]. We recently discovered that asTF induces angiogenesis, independent of PAR2 activation, by acting as an integrin ligand [16]. Thus, flTF and asTF facilitate cellular signaling via distinct mechanisms critical to tumor cell behavior.

Currently, nothing is known about asTF expression and function in breast cancer. Regulated splicing of TF pre-mRNA in human monocytes is controlled by several serine-rich (SR) proteins, including ASF/SF2 and SRp55 [17, 18]. Expression of SR proteins is frequently perturbed in BrCa tumors [2], and it is thus plausible that the relative abundance of flTF and asTF is also altered in BrCa.

Prior studies that attempted to correlate "TF expression" in BrCa specimens with clinical parameters, such as tumor grade and disease outcome, did not discriminate between flTF and asTF [19, 20]. Thus, there is uncertainty as to how the two TF isoforms associate with/contribute to BrCa progression. We set out to characterize flTF and asTF expression in a large set of BrCa tissue specimens. Identified associations were tested *in vitro* using innovative cell models, and *in vivo* with recapitulation of distinct BrCa subtypes.

Materials and Methods

Reagents. Full-length tissue factor (flTF)-specific antibody 10H10, protease activated receptor (PAR)-2, FVII(a)-, and the β1 integrin antibody AIIB2 were described previously [11]. p21 antibody, β1 integrin antibody (residues 579-799), β3 integrin-blocking antibody and HUTS-21(an antibody that recognizes the active conformation of β1 integrins) were from Millipore (Billerica, MA). Rabbit monoclonal antibodies against p27 and human alternatively spliced TF (asTF) (RabMab1, custom made) were from Epitomics (Burlingame, CA). p-MAP kinase/MAP kinase antibodies were from Cell Signaling Technologies (Beverly, MA). The β1 peptide was from Prospec-Tany Technogene (East Brunswick, NJ). flTF-specific antibody and asTF-specific rabbit polyclonal antibody used for immunohistochemistry were from American Diagnostica, [4509(main text Fig.1 legend)], (Stamford, CT) or described before [21], respectively. Mac3 and Ki67 antibodies were from BD Biosciences (San Jose, CA). Alexa-488 or Alexa-594-labeled antibodies were from Invitrogen (Carlsbad, CA).

Cell culture, transfections and viral transductions. All cells were cultured in DMEM (PAA, Cölbe, Germany) with 10% serum, 2 mM L-glutamine, penicillin and streptomycin. FRT sites were introduced to MCF-7 cells using Lipofectamine 2000 (Invitrogen, Carlsbad, CA). Cells were subsequently cultured in media containing 100 µg/ml zeocin, FRT insertion was verified by determining β-Galactosidase expression on Western Blot. FRT cell lines (2A3-3 and 2A1-2) were co-transfected with recombinase-encoding pOG44 and pcDNA5-FRT to produce control cells. Similar transfections were carried out with pcDNA5-FRT vector containing cDNA encoding flTF or asTF to produce TF variant-expressing cell lines. The cells undergoing homologous recombination were selected in media containing 150 µg/ml hygromycin. Transductions were carried out with shRNA lentiviral particles prepared from the Mission Library (Sigma-Aldrich, St. Louis, MO). Transduced cells were selected with 2 µg/ml puromycin.

Western Blotting. Cells were lysed in sample buffer (Invitrogen). Cell lysates or purified proteins were run on 8-16% gradient gels and transferred to PVDF membranes. Membranes were blocked in 5% non-fat milk powder and incubated with the appropriate primary antibodies, followed by HRP-conjugated secondary antibodies. Protein bands were visualized using Western Lightning ECL (PerkinElmer, Groningen, The Netherlands) and Kodak film (X-Sanatec, Roermond, The Netherlands).

Microarray analysis and validation. Total RNA was isolated, amplified and biotin labeled for hybridization on Illumina HumanHT-12 v4 Expression BeadChips using the Illumina Total Prep-96 protocol. Bioconductor (www.bioconductor.org) was used for the initial microarray analyses [22]. The 'lumi' library was used for loading and normalizing the Illumina arrays into R and Loess normalization was applied. A gene filter library was used for removing genes that did not show significant variations after normalization. Finally, the Limma library was used for performing three statistical comparisons: flTF vs. control, asTF vs. control, and asTF vs. flTF. Selected up-regulated or down-regulated were chosen, and expression levels were validated by real-time PCR. The primers are listed in table SII. The gene array data are accessible at Gene Expression Omnibus (accession no. GSE41872).

Soft agar growth assay.

Colony formation in soft agar was assayed by plating 10,000 cells in 0.6% agar/DMEM (wt/vol) on top of a 0.75% agar/DMEM layer in 35 mm dishes. Plates were incubated at 37˚C and 5% CO_2 for 14 days. Colonies were visualized using an inverted microscope (Leica DMIL) and Leica DFC295 camera. Cumulative colony size (area covered) and colony numbers were determined using ImageJ software.

Cell proliferation and apoptosis assays.

Cell proliferation was assessed using MTT assays as described previously [23]. In some experiments, outcomes of MTT assays were verified using cell counting and DNA analysis. In brief, cells were seeded in 10-cm dishes, lifted, and counted at day 0 and day 3. Proliferation was expressed as an increase in cell number compared with the cell number at day 0. For DNA analysis, cells were lysed in SDS buffer at day 0 and day 3 and DNA contents were measured using Nanodrop. When appropriate, flTF- (10H10, 50 μg/ml), asTF- (RabMab1, 50 μg/ml), β1- and β3 integrin antibodies (50 μg/ml) or a β1 peptide (1 nM) were added. To measure apoptosis, cells were lifted, incubated with Annexin V/propidium iodide (both Sigma-Aldrich, St. Louis, MO) and measured by FACS (LSR2; Becton Dickinson, Franklin Lakes, NJ)

Immunofluorescence studies.

For HUTS-21 staining, cells were fixed in methanol for 5 minutes. In all other experiments, cells were fixed in 2% (wt/vol) formaldehyde, permeabilized with 0.1% Triton-X100 when appropriate. Cells were incubated overnight with primary antibodies followed by incubation with secondary antibodies conjugated to Alexa-488 or Alexa-594. Coverslips were mounted using Vectashield containing DAPI (Vector Laboratories, Burlingame, CA). In some experiments, cells were incubated with fluorescently-conjugated asTF for 20 min, before fixation. Images were acquired using a Leica SP5 confocal microscope and a Leica DMI6000B.

Orthotopic breast cancer models and immunohistochemistry.

Animal experiments were approved by the animal welfare committee of the Leiden University Medical Center (LUMC). 5 animals per experimental group were used. The 2A3-3 cells ($2*10^6$ in 50 μl) were injected into the inguinal fat pad of NOD-SCID mice (Charles River, Wilmington, MA). Tumor growth was measured using calipers and the formula Volume=(length*width*width)/2. For MDA-MB-231-mfp growth *in vivo*, $0.5*10^6$ cells were injected in fat pads of NOD-SCID-gamma mice (Charles River). After completion of the experiment, mice were killed and tumors were extracted and fixed in 4% formalin. Sections were de-paraffinized, rehydrated and endogenous peroxidase activity was blocked with 0.3% H_2O_2. Antigen retrieval was done in sodium citrate buffer for 10 minutes at 100˚C. Sections were blocked with 10% normal goat serum in PBS and incubated overnight at 4 ˚C with primary antibody. Sections were incubated for 30 minutes with Envision (Dako, Heverlee, Belgium), visualized using DAB, and counterstained with hematoxylin.

Tissue microarray analysis.

A tissue array was constructed from tumor material obtained from 574 non-metastasized breast cancer patients that mostly underwent tumor resection at Leiden University Medical Center between 1985 and 1994 [24]. Approval was obtained from the LUMC Medical Ethics Committee. Age, tumor grade, histological type, tumor-node-metastasis status, median follow-up (17.9y), locoregional or distant tumor recurrence, and expression of estrogen receptor (ER), progesterone receptor (PgR), and human epidermal growth factor receptor 2 (HER2) were known. Tumors were graded according to the current pathological standards. Normal mammary tissue of 266 patients (46%) was available for analysis. Sections were cut and stained for flTF and asTF as described above. The percentage of asTF and flTF positive tumor cells was scored by two blinded observers. Patients in the 1^{st} quartiles were deemed negative.

Statistics.

Assessment of the associations between flTF/asTF expression and clinical variables were performed using SPSS and Stata. Cohen's κ coefficient for inter-observer agreement was 0.85 and 0.88 for asTF and flTF, respectively. The χ^2 test was used to evaluate associations between clinicopathological parameters and asTF/flTF expression. Analysis of *in vitro* and *in vivo* experiments was carried out using t-tests. Mean and SD are shown in figures, unless stated otherwise. Significant differences in bar graphs are indicated by * ($p<0.05$), ** (p,0.01) and *** (p,0.001).

Results

asTF expression positively correlates with BrCa grade and stage

Prior studies pointed to a potentiating role for TF in tumor progression [19, 20, 25]. To explore whether asTF and flTF differentially contribute to BrCa progression, we analyzed asTF and flTF protein expression in a BrCa tissue array comprising specimens from 574 BrCa patients [24]. asTF and flTF were detectable in >95% of the BrCa specimens with various degree of tumor cell positivity. Healthy mammary tissue showed far more limited expression of asTF compared with flTF (asTF: 4% of all specimens, flTF: 38%; **Fig. S1A)**. Specificity of previously validated flTF- and asTF-specific antibodies [21] was re-confirmed **(Fig. S1B)**. Confocal analysis revealed flTF localization on the cell membrane, while asTF was mostly intracellular **(Fig. S1C)**.

Expression of asTF positively correlated with histological grade as well as tumor size (Table I), but flTF expression only correlated with grade. asTF expression also correlated with age. No significant associations were found between asTF or flTF levels and estrogen

receptor (ER), progresterone receptor (PgR), or human epidermal growth factor receptor 2 (HER2) status. This finding raises the possibility that asTF impacts BrCa progression in a manner qualitatively distinct from that of flTF.

asTF expression enhances proliferation of BrCa cells

To explore the mechanistic link between the unique correlation of asTF expression and BrCa clinical parameters, we constructed MCF-7 cells harboring a genomic flippase recognition target (FRT) insertion, thus containing a unique locus-specific DNA acceptor site and established several FRT lines, selecting clone 2A3-3 for further studies. Insertion of asTF and flTF cDNA resulted in similar mRNA expression levels, but intracellular protein levels of asTF were lower **(Fig. S2A, S2B)**, likely because of asTF secretion (see below and **Fig. 1G**). Confocal analysis revealed that flTF was localized on the plasma membrane, confirmed by FACS analysis **(Fig. S2D)**, but asTF was present in vesicular structures (Fig. 1A). Only 2A3-3 flTF exhibited significant coagulant activity **(Fig. S2C)**. asTF protein levels were ~ fivefold higher in 2A3-3-asTF cell lysates than in lysates of tumor tissue-array specimens with high asTF positivity, likely because of the constitutive asTF overexpression of 2A3-3 cells and the appreciable presence of asTF-negative stroma (upto 50%) in our tumor specimens **(Fig. S2E)**. The 2A3-3 cells expressing flTF, asTF, an aspecific protein (β-Galactosidase), or empty vector control cells (pcDNA) were tested in an MTT proliferation assay and compared with parental MCF-7 cells. The 2A3-3-pcDNA and 2A3-3-βGal proliferation rates were identical to those of MCF-7 **(Fig. 1B)**, but proliferation rates of 2A3-3-asTF cells were increased by ≥twofold, while those of 2A3-3-flTF cells were only modestly increased. Cell counting and genomic DNA measurements confirmed these results **(Fig. S3A, S3B)**. An independently established second 2A3-3-asTF line showed similar proliferation rates **(Fig. S3C)** and TF-specific shRNA eliminated enhanced proliferation **(Fig. 1C,D)**, confirming that the effect was asTF-dependent. Because asTF contains an unusual C terminus as a result of a frameshift, a possibility exists that asTF expression may increase cell proliferation through activation of the unfolded protein response. However, we found no evidence for unfolded protein response activation or protein aggregation, neither in flTF-nor in asTF- expressing cells **(Fig. S3D, S3E)**. Increased cell numbers were also not a result of increased cell survival, as all cell lines exhibited similar viability levels **(Fig. S3F)**.

asTF and flTF expression resulted in down-regulation of cell cycle inhibitors and enhanced phosphorylation of the pro-mitogenic p42/p44 MAP kinase **(Fig. 1E)**. Effects of flTF and asTF expression on proliferation were somewhat less pronounced in an MCF-7 FRT clone (2A1-2) with lower flTF/asTF expression **(Fig. 1F,G and Fig. S3G)**. The 2A1-2 cells exhibited decreased asTF secretion but intracellular asTF levels were equal to those in 2A3-3 cells

(Fig. 1G), suggesting that asTF secretion is important to the enhancement of proliferation. Indeed, co-culture of control cells with asTF-expressing cells increased the proliferation of control cells **(Fig. 1H)**. Culturing control cells in 2A3-3-asTF-conditioned medium enhanced proliferation, and asTF depletion from the medium reversed this effect **(Fig. S4A)**. Addition of recombinant asTF to pcDNA cells increased proliferation at concentrations as low as 1nM, well below asTF concentrations detectable in the plasma of metastatic breast cancer patients **(Fig. S4B, S4C)**. Incubation of asTF-expressing 2A3-3 cells with an asTF-blocking antibody, but not with an flTF-blocking antibody, reduced asTF-dependent cell proliferation **(Fig. 1I)**. Limited flTF-elicited proliferation was not dependent on PAR2 activation, as incubation with PAR2, as incubation with PAR2- and FVII- blocking antibodies was without effect **(Fig. S4D)**. These results demonstrate that secreted asTF enhances BrCa cell proliferation in an autocrine fashion.

asTF augments pro-oncogenic gene expression

We compared gene expression profiles in asTF-expressing 2A3-3 cells with those in 2A3-3-pcDNA- or flTF- expressing 2A3-3 cells. Compared with 2A3-3-pcDNA or flTF- expressing cells, asTF expression up-regulated genes involved in cell cycle progression [e.g. cyclin A1 (*CCNA1*)], tumor proliferation [e.g. midkine (*MDK*)], cytoskeletal reorganization/motility [e.g. fermitin family homolog 2 (*FERMT2*)], invasion [e.g. family with sequence similarity 5, member C (*FAM5c*)], and cell survival [e.g. mesothelin (*MSLN*)] **(Fig. 2A,B)**. Moreover, expression of asTF down-regulated several tumor suppressors [e.g. cadherin 18) (*CDH18*)], and genes involved in cell cycle arrest [e.g. EGF containing fibulin-like extracellular matrix protein 1 (*EFEMP1*)] and apoptosis [DNA- damage regulated autophagy modulator 1 (*DRAM1*)] **(Fig. 2A,B** and Table S1). Expression of SRSF protein kinase 2 (SRPK2), which activates the TF pre-mRNA splicing regulator ASF/SF2 [26], was altered by asTF and flTF, suggesting that TF splice variants may regulate their own expression. These results indicate that asTF enhances BrCa cell proliferation via modulation of cell cycle regulators, proliferation inducers, and tumor suppressors/pro-apoptotic proteins.

asTF enhances proliferation by binding to β1 integrins

Because asTF induces angiogenesis via binding integrins on endothelial cells [16], we reasoned that asTF-dependent BrCa cell proliferation may also be integrin-dependent. Silencing of the β1 integrin subunit resulted in diminished proliferation of 2A3-3-asTF cells **(Fig. 3A and Fig. S5A)** and flTF cells **(Fig. S5A, S5B)**, but not 2A3-3-pcDNA cells; shRNA silencing of the β3 integrin subunit, which is not expressed in these cells, was without effect (Fig. S5C).

Artificially truncated recombinant flTF ("sTF") was recently found to induce EC proliferation by binding to the integrin β1 region between aminoacid residues 579 and 799 [27]. Because sTF contains the entire N-terminal region of asTF, we tested whether asTF binds to this integrin region. A β1 579-799 aa domain specific antibody and a peptide mimicking this domain inhibited proliferation of 2A3-3-asTF , but not control cells or 2A3-3-flTF cells even after prolonged incubation **(Fig. S5D, S5E)**. Co-immunoprecipitation (IP) demonstrated that asTF directly binds to β1 integrin and binding was lost after preincubation with the β1 579-799 aa antibody **(Fig. 3B)**. Binding of asTF to β1 integrins was confirmed using a modified ELISA showing that asTF binds well to recombinant α6β1 **(Fig. S5F)** which is consistent with our earlier findings [16]. Pre-incubation of control cells in suspension with recombinant asTF enhanced cell binding to collagen and fibronectin, but not vitronectin **(Fig. S5G)**, indicating that asTF binding may modulate integrin activation. Functional blockade of β1 reversed this effect **(Fig. 3C)**. In support of an activating effect of asTF on β1 integrins, reactivity of HUTS-21, an antibody that recognizes the active conformation of β1 integrins, increased when 2A3-3 cells expressed asTF or were exposed to recombinant asTF **(Fig. 3D)**. To ascertain asTF co-localization with β1 integrins, we pre-incubated pcDNA cells with fluorescently-tagged asTF; partial co-localized with β1 integrins on the cell surface was observed **(Fig. S5H)**. Because β1 integrin blockade in 2A3-3 cells only partially inhibited asTF-dependent proliferation, these results suggest that, aside from β1 integrins, asTF likely binds to other membrane-associated proteins.

asTF induces anchorage-independence and tumor growth *in vivo*

We next investigated the effects of asTF expression on oncogenic potential using soft-agar assays. Although, asTF did not affect the number of colonies, it caused a threefold increase in colony size; the impact of flTF expression on colony size was marginal **(Fig. 4A, 4B)**.

asTF-dependent tumor growth was then assessed orthotopically. asTF expression increased tumor expansion **(Fig. 4C)**, but flTF-expressing 2A3-3 cells yielded tumors that were similar in size or smaller than those formed by control cells. asTF-expressing cells yielded large tumors with little stroma, whereas control and flTF cells gave rise to small tumor islands surrounded by stroma **(Fig. S6)**. flTF and asTF protein expression was confirmed in tumors *in vivo*, ruling out that poor growth of flTF-expressing cells was because of loss of flTF expression **(Fig. S6)**. asTF-expressing tumors had more CD31+ capillaries and macrophage infiltrate, and contained more proliferating tumor cells, specifically at the tumor periphery **(Fig. 4D, 4E)**. These data demonstrate that asTF promotes BrCa cell proliferation *in vitro* and *in vivo*.

asTF blockade reduces growth of BrCa cells expressing endogenous asTF

Although we dissected the role of asTF in tumor growth using MCF-7 cells constructed to express either asTF or flTF, native asTF is co-expressed with flTF. Moreover, MCF-7 cells express low levels of PAR2, which may mechanistically explain the lack of 2A3-3-flTF-dependent tumor expansion *in vivo*. Because MDA-MB-231 BrCa cells express high levels of flTF and PAR2[11], we used them to assess the role of asTF in an flTF/PAR2-positive setting. Although asTF levels in MDA-MB-231 cells were low **(Fig. 5A)**, a more aggressive MDA-MB-231 sub-line that had been isolated from the mammary fat pad following orthotopic implantation (MDA-MB-231-mfp) [28] had significantly higher asTF levels, but flTF levels were unchanged. In agreement, spliceosomal proteins that promote biosynthesis of asTF mRNA were upregulated in MDA-MB-231-mfp cells **(Fig. S7A)**. Importantly, asTF levels in these cells were lower or equal to the asTF levels in BrCa specimens **(Fig. S2E)**. asTF-specific antibody blockade significantly inhibited proliferation of MDA-MB-231-mfp cells **(Fig. 5B)**, but had no effect on proliferation of the parental MDA-MB-231 line, demonstrating functional specificity. Selective anti-flTF antibody 10H10 did not inhibit proliferation of either cell type *in vitro*, which is consistent with the notion that flTF potentiates angiogenesis – but not proliferation – in these cells [11] **(Fig. 5B)**. A β1 integrin-blocking antibody and the 579-799 aa integrin peptide also inhibited proliferation of MDA-MB-231-mfp cells, but did not further reduce proliferation in the presence of the anti-asTF antibody **(Fig. 5C)**, confirming that asTF augments proliferation in MDA-MB-231-mfp via β1 integrins. The β3 integrin blockade was without effect **(Fig. 5D)**.

We then implanted MDA-MB-231-mfp cells orthotopically in NOD-SCID gamma (NSG) mice in the presence or absence of asTF-blocking antibody. asTF blockade with as little as 100 μg antibody significantly inhibited tumor growth **(Fig. 5E)** and resulted in a marked reduction of the proliferation zone at the tumor periphery **(Fig. 5F and Fig. S7B)**. Notably, asTF blockade did not reduce vascular density, suggesting that asTF does not impact angiogenesis in a model featuring a pro-angiogenic flTF-PAR2 axis **(Fig. 5G, and Fig. S7B)**. Thus, asTF blockade decreases the tumorigenic potential of BrCa cells expressing native asTF, flTF, and PAR2.

Discussion

Until now, contributions of asTF to tumor progression have remained unclear. This study is unique in reporting: i) asTF's selective abundance in BrCa tissue; ii) asTF-dependent, autocrine augmentation of BrCa cell proliferation; and iii)the efficacy of anti-asTf monoclonal antibodies in stemming BrCa growth. Analysis BrCa specimens from 574

patients revealed that asTF positively correlates with both grade and the T-status of cancer lesions, as well as the patients' age, but flTF correlates solely with tumor grade, and is detectable in ~40% of normal breast tissue, compared with ~4% for asTF. We demonstrate herein that asTF up-regulates BrCa cell proliferation irrespective of its impact on angiogenesis in an asTF overexpression model, as well as in BrCa cells that express native asTF.In contrast to asTF-triggered proliferation, flTF-triggered proliferation rates were low in our TF overexpressing cells. Furthermore, flTF-dependent proliferation was not observed in an aggressive MDA-MB-231 cell line that expresses asTF. Thus, asTF appears to be the major TF variant that promotes BrCa cell proliferation.

asTF upregulated genes that play pivotal roles in cell cycle progression and proliferation. *CNNA1* and *CNNA2*, important regulators of cyclin-dependent kinases during S phase, and anaphase promoting complex 10 (*ANAPC10)* were significantly up-regulated in 2A3-3-asTF cells compared with control or flTF expressing cells. Growth factors [*MDK*, *GAL* and tissue inhibitor of metalloproteinases 1(*TIMP1)*] were also up-regulated. Alhough we observed up-regulation of some cell survival genes, we found no evidence for altered cell survival in asTF-expressing cells. Still, it cannot be ruled out that these genes contribute to the cumulative impact of asTF expression on tumor xenografts.

Our studies further revealed that asTF-integrin interactions were responsible for increased proliferation of BrCa cells. asTF co-localized with and bound to β1 integrins and β1 integrin silencing reversed asTF dependent proliferation. Anantibody against the β1 region encompassing residues 579-799 or a peptide mimicking this domain, reversed asTF-dependent – but not flTF-dependent – proliferation, indicating that asTF binds to this distinct β1 region. We hypothesize that asTF induces a conformational change in β1 integrins that render them prone to activation, as we used a β1 integrin-blocking antibody that is reactive with the membrane-proximal β-tail domain (βTD) of the β1 integrin subunit, and the 579-799 integrin peptide features this domain. The βTD contains a CD-loop that contacts the ligand-binding integrin βA domain and the hybrid domain, and this contact is lost upon integrin activation [29, 30]. It has been postulated that the CD-loop acts as a deadbolt, preventing integrin activation by locking βA in an inactive state. Indeed, a number of antibodies that activate β1 integrins bind to the βTD or the βA interface, and the βTD has been shown to regulate ligand binding [29, 31]. We propose that asTF induces removal of the CD-loop deadbolt. However, direct conformational effects of asTF on of β1 integrin function may not be the sole means by which asTF modulates the "integrin profile" of BrCa cells: asTF expression also up-regulates kindlin-2, a positive regulator of talin-induced integrin activation [32], and suppresses tensin-3, a negative regulator of integrin function [33].

The *in vitro* phenotype of asTF-expressing 2A3-3 cells, (enhanced proliferation and colony growth in soft agar colony growth), was recapitulated *in vivo* but flTF-expressing cells that proliferated only moderately faster than control cells *in vitro*, produced tumors of the same size as control cells. It is not clear why flTF overexpression in MCF-7 cells did not enhance tumor growth *in vivo*, but the paucity of PAR2 expression may be a contributing factor. PAR2 is instrumental in flTF-dependent tumor angiogenesis [11], and poor expansion of these cells may result from a lack of PAR2-dependent angiogenesis. This finding is in agreement with the results of *in vivo* experiments using PAR2-expressing MDA-MB-231-mfp cells: asTF blockade did not affect vascular development in tumor xenografts, although we did not directly test the influence of asTF-induced angiogenesis on BrCa growth. Our results indicate that asTF does not significantly influence angiogenesis in the MDA-MB-231-mfp xenograft model, while upregulation of CD31+ vessels in asTF-expressing 2A3-3 tumors suggests that asTF-dependent angiogenesis may be a contributing factor in 2A3-3 xenografts. Differences in secreted asTF levels and presence of a functional flTF-PAR2 axis in MDA-MB-231-mfp cells may explain why asTF differently affects vascular density in these two xenograft models.

Alternative splicing has been deemed critical to the proliferation of BrCa cells: overexpression of ASF/SF2, a major SR protein and regulator of the flTF/asTF mRNA ratio in monocytes [18], leads to enhanced proliferation, transformation, and BrCa growth *in vivo* [1]. Furthermore, the expression of SRp40 – the spliceosomal protein that promotes asTF synthesis [17], the levels of which are up-regulated in MDA-MB-231-mfp cells – is increased in human BrCa, and associated with lymph node metastasis [34]. It may be of interest to investigate whether the effects of heightened SRp40 expression in BrCa are in part dependent on asTF production.

In conclusion, autocrine asTF expression induces integrin-mediated BrCa cell proliferation that contributes to tumor growth, rendering asTF a unique target for anti-cancer strategies that modulate the biological activity of this minimally coagulant TF form, thereby avoiding adverse impacts on hemostasis.

Characteristic	Total N (%)	asTF- N (%)*	asTF+ N (%)*	P	flTF- N (%)*	flTF+ N (%)*	P
Total	574 (100)	119 (100)	328 (100)		157 (100)	351 (100)	
Age (y)							
<40	48 (8.4)	5 (4.2)	26 (7.9)		15 (9.6)	26 (7.4)	
40–60	277 (48.3)	72 (60.5)	153 (46.6)	0.03	75 (47.8)	171 (48.7)	0.71
≥60	249(43.4)	42 (35.3)	149 (45.4)		67 (42.7)	154 (43.9)	
Missing*	0 (0.0)	0 (0.0)	0 (0.0)		0 (0.0)	0 (0.0)	
Grade							
I	81 (14.1)	26 (21.8)	28 (8.5)		30 (19.1)	41 (11.7)	
II	282 (49.1)	58 (48.7)	159 (48.5)	<0.001	88 (56.1)	157 (44.7)	<0.001
III	203 (35.4)	33 (27.7)	138 (42.1)		35 (22.3)	149 (42.5)	
Missing*	8 (1.4)	2 (1.7)	3 (0.9)		4 (2.5)	4 (1.1)	
Histotype							
Ductal	514 (89.5)	104 (87.4)	300 (91.5)		133 (84.7)	320 (91.2)	
Lobular	53 (9.2)	13 (10.9)	25 (7.6)	0.39	20(12.7)	27 (7.7)	0.065
Missing*	7 (1.2)	2 (1.7)	3 (0.9)		4 (2.5)	4 (1.1)	
T status							
T1	211 (36.8)	56 (47.1)	97 (29.6)		64 (40.8)	120 (34.2)	
T2	272 (47.4)	46 (38.7)	173 (52.7)	0.002	71 (45.2)	171 (48.7)	0.26
T3–4	72 (12.5)	13 (10.9)	49 (14.9)		17 (10.8)	51 (14.5)	
Missing*	19 (3.3)	4 (3.4)	9 (2.7)		5 (3.2)	9 (2.6)	
N status							
N0	307 (53.5)	64 (53.8)	166 (50.6)		93 (59.2)	182 (51.9)	
N1–3	250 (43.6)	53 (44.5)	153 (46.7)	0.62	62 (39.5)	158 (45.0)	0.18
Missing*	17 (3.0)	2 (1.7)	9 (2.7)		2 (1.3)	11 (3.1)	
ER status							
Negative	208 (36.2)	37 (31.1)	124 (37.8)		54 (34.4)	123 (35.0)	
Positive	344 (59.9)	79 (66.4)	193 (58.8)	0.17	93 (59.2)	214 (61.0)	0.96
Missing*	22 (3.8)	3 (2.5)	11 (3.4)		10 (6.4)	14 (4.0)	
PgR status							
Negative	234(40.8)	40 (33.6)	136 (41.4)		50 (31.8)	144 (41.0)	
Positive	311(54.2)	77 (64.7)	181 (55.2)	0.10	97 (61.8)	191 (54.4)	0.06
Missing*	29 (5.1)	2 (1.7)	11 (3.4)		10 (6.4)	16 (4.6)	
HER2†							
Negative	406 (70.7)	86 (72.3)	236 (71.9)		105 (66.9)	244 (69.5)	
Positive	50 (8.7)	6 (5.0)	32 (9.8)	0.14	9 (5.7)	32 (9.1)	0.28
Missing*	118 (20.6)	27 (22.7)	60(18.3)		43 (27.4)	75 (21.4)	

Table I. Association of asTF and flTF with patient and tumor characteristics

*During specimen processing, some tumor punches were lost leading to a smaller patient number per staining. P-values were calculated based on the remaining specimens. **HER2 status was not known for all patients

Abbreviations: asTF, alternatively spliced tissue factor; flTF, full length tissue factor; T, tumor; N, Axillary lymph node; ER, estrogen receptor; PgR, progesterone receptor; Her2, human epidermal growth factor 2.

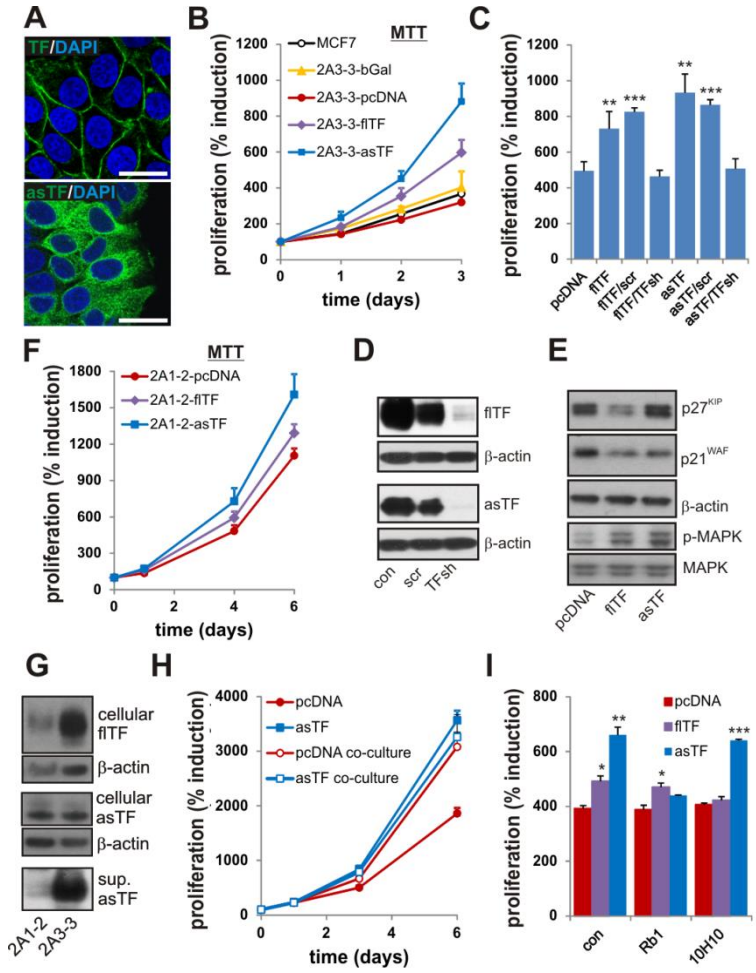

Figure 1. asTF expression induces cancer cell proliferation. (A) FRT cells (clone 2A3-3) received flTF or asTF cDNA by homologous recombination. Localization of flTF (upper) and asTF (lower) was assessed by confocal microscopy using specific antibodies [monoclonal flTF-specific Ab 4509 and polyclonal asTF-specific Ab, as described previously [21]). Scale bars: 25 µm. (B) Proliferation of 2A3-3 cells containing the cDNAs indicated was monitored using MTT assays. (C) 2A3-3-flTF or 2A3-3-asTF were transduced with TF-specific or control shRNA. Cells were subjected to MTT assays 3 days after the start of the experiment. (D) flTF and asTF expression in 2A3-3 cells transduced with TF-specific or control shRNA constructs. (E) Expression of cell cycle inhibitors and MAP kinase phosphorylation was assessed in 2A3-3 cell lines. (F) Cell line (2A1-2) harboring an FRT site at a transcriptionally less active region received empty vector, flTF or asTF cDNA and proliferation was monitored using MTT assay. (G) Cell associated and secreted levels of asTF and flTF in 2A3-3 and 2A1-2 cells. (H) pcDNA cells and asTF-expressing cells were grown separately, or in adjoining 12-well plates containing an open port, allowing asTF diffusion to control cells. Proliferation was monitored using MTT assay. (I) 2A3-3-pcDNA, 2A3-3-flTF, or 2A3-3-asTF cells were treated with 50 µg/ml flTF-signaling blocking antibody (10H10) or asTF-blocking antibody (RabMab1,Rb1), proliferation was assessed 3 days later using MTT assay. *P<0.05, **P<0.01, ***P<0.001.

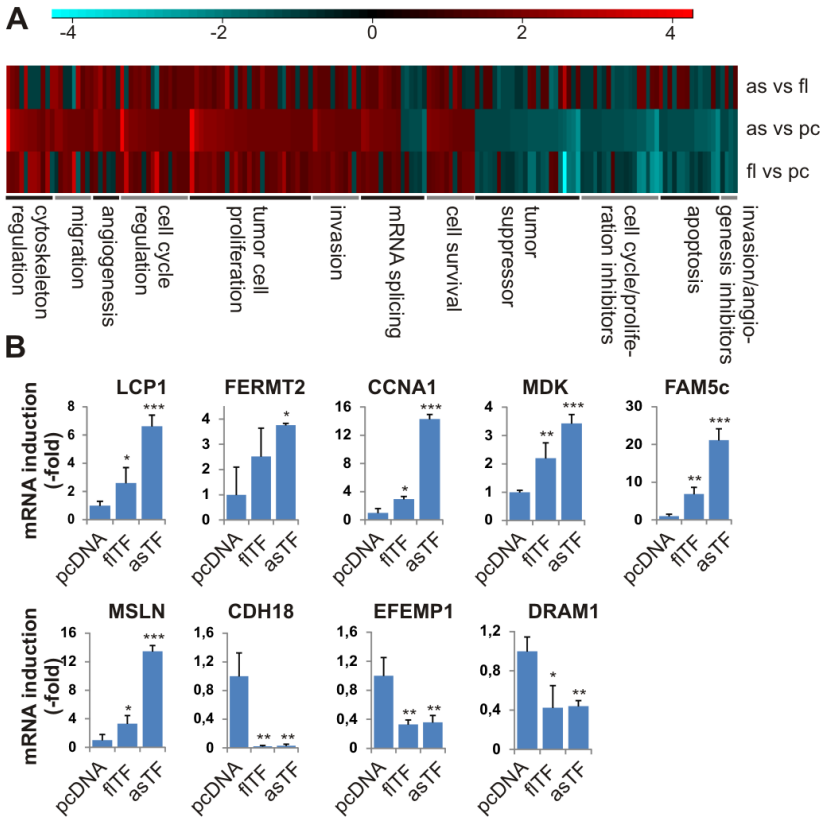

Figure 2. Microarray analysis of flTF and asTF expressing cells. (A) Heat map representation of relevant genes in flTF and asTF expressing 2A3-3 cells, compared with control. The heat map comprises the genes whose expression was significantly up- or down-regulated ($P<0.05$) by at least 1.33-fold. Results of 4 independent experiments are shown; red and blue denote up- and down-regulation, respectively. (B) Up-regulation of selected genes was verified using real-time PCR.

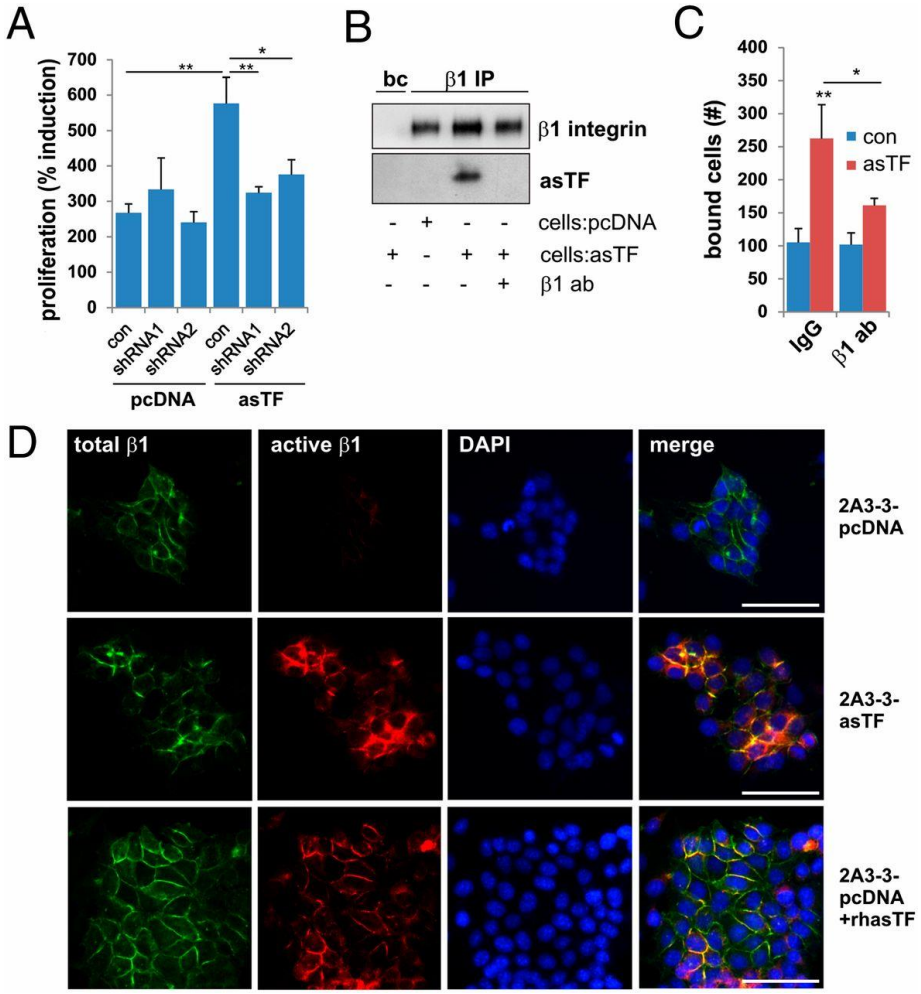

Figure 3. TF variant-induced proliferation is integrin dependent. (A) pcDNA control cells or asTF-expressing 2A3-3 cells were transduced with shRNA to silence β1 integrins, and proliferation of these cells was compared to with after 3 days. (B) 2A3-3-pcDNA or –asTF cells were mock-treated or incubated with a β1 (epitope 579-799) –reactive antibody. The cells were lysed in Brij78-containing lysis buffer and β1 integrin was precipitated using AIIB2. asTf co-immunoprecipitation was assessed by western blot. (C) 2A3-3-pcDNA cells were preincubated with 10 nM recombinant asTF in the presence or absence of an antibody against β1 integrin epitope 579-799 and seeded on collagen I. After washing remaining cells were counted. (D) 2A3-3-asTF cells or 2A3-3-pcDNA cells, untreated or incubated with 10 nM recombinant asTF, were fixed and stained with AIIB2 (total β1 integrin; green) and HUTS-21 (activated β1 integrin; red). Scale bars: 50 µm. *P<0.05, **P<0.01, ***P<0.001.

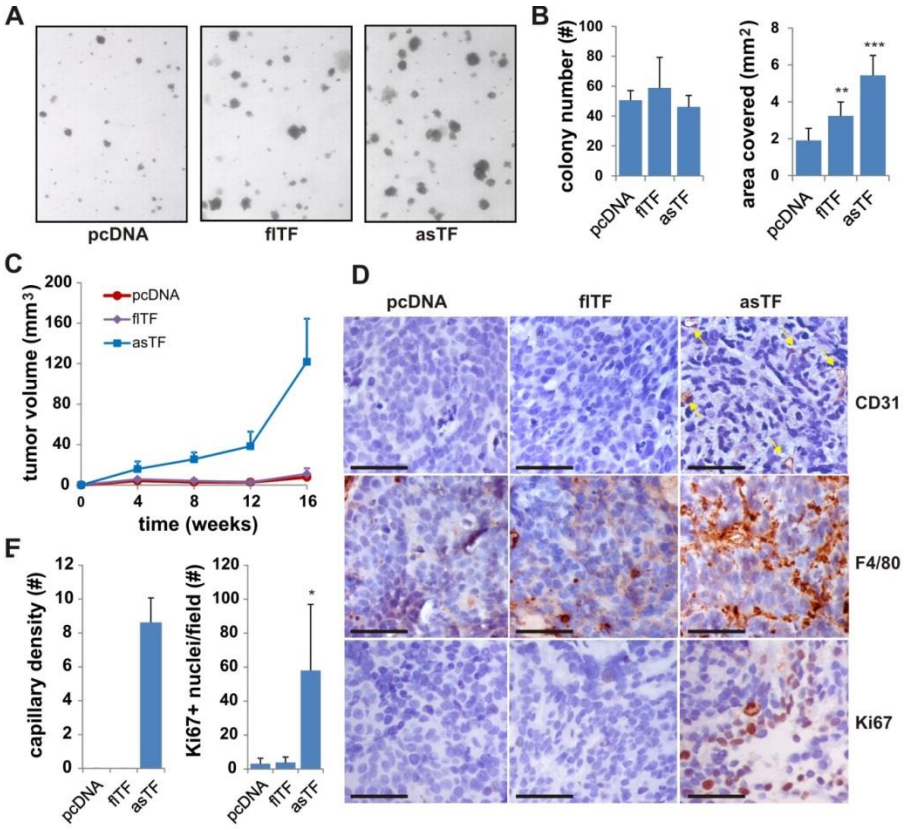

Figure 4. TF variant-induced transformation and tumor growth. (A) 2A3-3-pcDNA, flTF or asTF cells were seeded in soft agar and allowed to grow for 14 days. Images were captured and colony number per area covered determined using ImageJ (B). (C) 2A3-3-pcDNA, flTF or asTF cells were injected into the mammary fat pad of NOD-SCID mice, and tumor growth assessed for 16 weeks. Mean and SEM are shown. (D) Tumors were analyzed by immunohistochemistry to assess vascular density (CD31), macrophage infiltration (Mac3), and proliferation rate (Ki67). Scale bars represent 50 μm. (E) Quantification of vascular structures per view field.

*P<0.05, **P<0.01, ***P<0.001

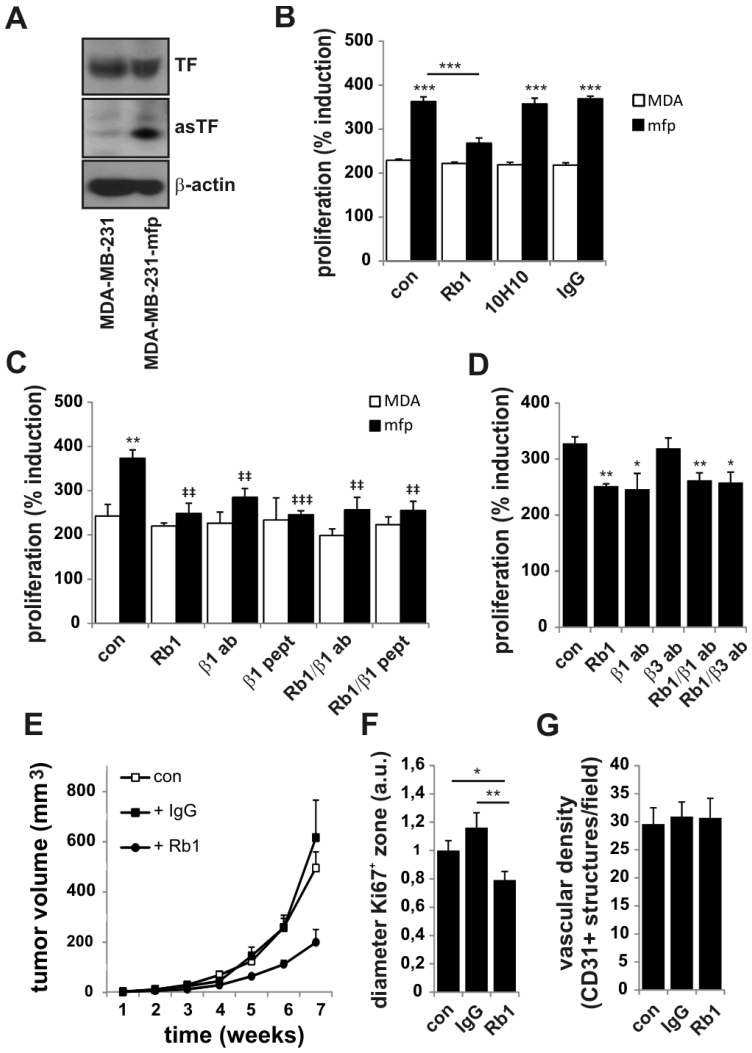

Figure 5. asTF induces tumor cell proliferation of BrCa cells endogenously expressing flTF/asTF/PAR2. (A) flTF and asTF expression in MDA-MB-231 and MDA-MB-231-mfp cells. β-actin is used as a loading control. (B) MDA-MB-231 (MDA) and MDA-MB-231-mfp (mfp) cells were grown in the presence of asTF-specific antibody (Rb1), flTF-specific antibody 10H10, or IgG control. Proliferation was assessed after 3 days using MTT assay. (C) As in B, but blocking antibodies against β1 integrins or the β1 peptide was added separately or in combination with Rb1. * indicates significant differences compared to control (MDA-MB-231) cells, *P<0.05, **P<0.01, ***P<0.001. ‡ indicates significant differences compared with MDA-MB-231-mfp cells (D) As in B, a β3-blocking antibody was added. (E) MDA-MB-231-mfp cells were injected in the mammary fat pad of NOD-SCID-gamma (NSG) mice in the presence or absence of 100 μg Rb1 or IgG control. Mean tumor volume and SEM are shown. (F) Tumor specimens were stained with anti-Ki67, and the proliferation zone diameter (Ki67+ area at the periphery of the tumor) was determined. Values are expressed as arbitrary units, with the control set at 1. (G) Quantification of $CD31^+$ structures in the tumor specimens shown in F.

Table SI. List of genes included in the heatmap in Fig.2A

gene	asTF vs control	p-value	flTF vs control	p-value
cytoskeleton regulation				
LCP1	3,742041408	4,82E-07	1,597922314	0,004017
SCIN	2,108646599	7,30E-09	1,329457586	0,000118
TUBB2B	1,928582645	0,000285	1,477838294	0,010475
CORO1A	1,868572756	8,27E-06	2,14044709	1,17E-06
UBE2L6	1,780560434	0,000203	2,210948723	1,14E-05
RDX	1,749752453	1,33E-06	-1,313590672	0,000873
HAX1	1,7014436	1,56E-05	2,036833659	8,66E-07
LOC606724	1,635658577	4,22E-05	2,067936846	9,50E-07
STMN3	1,470501982	0,001837	1,852729618	3,99E-05
TWF1	1,390079424	1,38E-05	1,047946252	0,326043
RHOD	1,398217432	0,001541	-1,418470373	0,001135
integrin and migration				
BGN	1,859405347	0,000335	-1,049253889	0,703295
FERMT2	1,857779519	2,67E-06	1,193333563	0,032271
SMAGP	1,530149351	7,72E-05	1,574769438	4,29E-05
TRIP6	1,433852054	8,72E-06	1,447503733	6,78E-06
ID1	1,429662141	0,024691	2,92285299	6,89E-06
TM4SF1	1,422992101	0,041298	-1,623238739	0,008735
ZFYVE21	1,408507583	1,50E-06	1,303102493	1,87E-05
ITGAE	1,370217825	1,44E-05	-1,093804744	0,064612
RAPGEF2	1,341491552	3,69E-06	1,019520069	0,597044
angiogenesis inducer				
CTSH	2,078278757	1,30E-06	1,227613867	0,025359
PTGES	1,804505885	1,98E-05	-1,16678851	0,095746
METAP1	1,451736383	4,43E-06	1,279896922	0,000197
HIF1A	1,442084355	0,000576	-1,069079685	0,407952
NCL	1,42837763	0,000151	-1,02074889	0,755335
PLA2G3	1,34121158	8,50E-06	1,361032506	5,28E-06
cell cycle				
CCNA1	3,444212992	1,03E-09	1,311815883	0,00223
TEAD2	1,999153596	0,001922	2,719114401	0,000105
CCNA2	1,689827846	1,02E-07	1,351804407	2,68E-05
ANAPC10	1,684016033	9,30E-08	1,174051955	0,003684
MAD2L1	1,584491419	1,23E-05	1,192226934	0,017

CBL	1,506003722	0,000116	-1,00792761	0,914163
CDC5L	1,45321681	0,001637	1,130303557	0,205681
ID3	1,444140914	0,021992	1,864606082	0,000831
ID1	1,429662141	0,024691	2,92285299	6,89E-06
PIR	1,376465624	2,23E-05	1,146793418	0,012949
LIN54	1,373650529	0,000956	1,261968371	0,007639
MNAT1	1,37187435	0,002633	-1,05517336	0,528861
LCMT1	1,368999315	0,000314	1,35855059	0,000383
MRS2	1,360460762	1,16E-05	1,079358084	0,094399
NUP153	1,351409693	0,000212	1,077304377	0,213649
GMNN	1,344105524	0,008987	1,090079751	0,37861
tumor cell proliferation				
H19	3,489019144	2,00E-12	2,954286767	1,01E-11
MDK	2,454063596	2,31E-05	1,387160376	0,029261
GAL	2,037698068	0,000246	1,512087264	0,010815
PCSK1N	1,862575221	1,26E-06	1,567716533	2,98E-05
MND1	1,860190359	6,09E-07	1,438271735	0,000105
ODC1	1,834345353	1,52E-06	1,81512049	1,82E-06
SLC16A3	1,761121624	0,000333	1,313471999	0,032633
TIMP1	1,760619541	0,000204	1,180564302	0,143626
TBX2	1,658101848	0,000721	-1,381987092	0,013261
PHF19	1,647718256	3,45E-05	1,488760883	0,000253
MAPK13	1,536585166	0,000472	2,035143814	5,15E-06
FABP5	1,532500067	1,20E-07	1,384337539	2,01E-06
EIF4E	1,547804854	0,001	1,020291222	0,843895
PFKM	1,481369052	0,000113	1,731273689	5,05E-06
HOXB7	1,463554404	4,50E-05	1,147175144	0,041784
FGFR3	1,462154414	0,000446	1,341156069	0,002959
MARCKS	1,423358397	0,002797	-1,297591069	0,016804
PRR5	1,422956559	0,000163	1,159269894	0,041068
RAP1GDS1	1,417514749	4,30E-06	1,186787763	0,00195
PPIL1	1,416748859	0,00359	1,195002505	0,087845
PFKP	1,409792362	1,42E-05	1,502888233	2,68E-06
ATOX1	1,405348878	0,000415	2,200283203	1,38E-07
YWHAG	1,400002412	0,000612	1,006903933	0,925548
PLOD3	1,386953228	0,002265	1,22269681	0,034265
PBK	1,362937947	0,00072	1,537087528	4,54E-05

RAP1GDS1	1,347424073	2,88E-06	1,060408762	0,1227
FDFT1	1,344708736	0,134579	1,046267955	0,810124
CALM1	1,341930602	0,000384	1,342218442	0,000381
Invasion				
FAM5C	2,092361538	7,64E-09	1,408929672	2,08E-05
LMO4	1,539098114	1,30E-05	1,395712469	0,000135
ACSL4	1,475175376	1,28E-07	1,333133311	2,87E-06
HMGN5	1,451825346	2,79E-05	1,262108012	0,001409
FGFR4	1,418287964	9,36E-05	1,629394916	4,06E-06
MMP9	1,383610445	1,05E-05	1,308708358	6,07E-05
CUX1	1,383282194	0,00048	1,223505839	0,011696
EGR3	1,354850524	0,002475	1,069302011	0,412034
PTTG1	1,341683457	0,000607	1,656079806	4,92E-06
SEMA3E	1,332027901	0,243818	-1,383155273	0,190906
SMAGP	1,330776688	0,00024	1,415029063	4,39E-05
mRNA splicing				
HNRNPH1	1,928871989	0,000228	1,238105925	0,1129
SNRPC	1,82563735	3,20E-06	1,445397593	0,000289
HNRPDL	1,572832064	9,64E-05	1,353544414	0,002292
HNRNPH3	1,509978879	3,07E-05	1,309311687	0,001083
HNRNPU	1,508793814	0,026946	-1,161521139	0,374949
LSM6	1,485474582	0,003655	1,017512615	0,875937
SRPK1	1,437383427	9,62E-05	1,053853601	0,415897
SNRPC	1,42544196	0,000444	1,353365203	0,001476
PRCC	1,361638994	0,001173	1,226295917	0,015717
THOC5	-1,331761098	0,000936	-1,01730332	0,796002
KHSRP	-1,357140125	0,002549	1,16120239	0,085754
SNRPD3	-1,391235152	2,91E-05	-1,149889184	0,016124
LSM14A	-1,412268479	3,25E-05	-1,276059742	0,000633
TTF2	-1,423558516	0,000219	-1,07828293	0,280668
SRPK2	-1,899174927	1,74E-05	-1,800406495	3,90E-05
cell survival				
MSLN	1,759854431	5,95E-07	1,142949637	0,038443
GPX3	1,673571357	1,79E-05	1,252757581	0,010156
GPX8	1,644675123	3,80E-07	1,352780874	5,08E-05
UBE2D3	1,52981016	5,55E-05	1,438741757	0,000216
LAMTOR3	1,520041452	8,40E-08	1,178291252	0,000614

SIVA1	1,403788792	0,000222	1,602042598	1,15E-05
BCAS2	1,365068982	0,066403	-1,27417534	0,141433
RBM38	1,362618327	0,005194	1,098192724	0,318759
HMGA1	1,35714425	0,088863	1,393404303	0,067435
WBSCR22	1,342446449	0,000828	1,465913378	9,70E-05
IER3	1,333800324	0,082352	1,506736772	0,019669
tumor suppressor				
MB	-1,33064222	0,00093	-1,446513458	0,000116
CDH1	-1,332727303	0,00057	-1,202639385	0,011018
STAT1	-1,339818537	5,97E-06	-1,400991988	1,45E-06
PLK2	-1,367464292	4,18E-05	-1,37124953	3,86E-05
CCDC6	-1,370125987	4,79E-05	-1,254761305	0,000751
LRRC26	-1,372949147	7,11E-05	1,170114234	0,011712
ENO1	-1,375689186	3,63E-05	-1,074586971	0,169045
PRDM4	-1,378877472	0,001111	-1,045399441	0,562209
RND3	-1,393657887	0,001223	-1,022880967	0,776587
KLF6	-1,411761734	9,31E-05	-1,331647695	0,000442
PPP1R7	-1,423655222	4,41E-06	-1,39691304	7,57E-06
SSBP2	-1,448869666	7,34E-07	-1,110176831	0,018871
PTPRK	-1,500527266	9,46E-06	-1,954301708	5,54E-08
RPRM	-1,509953249	1,68E-05	-1,921471447	1,62E-07
LZTR1	-1,517064516	0,002917	-1,191377647	0,140816
PCDH19	-1,524311442	1,20E-05	-1,593325281	4,53E-06
DNAJB6	-1,556756399	1,40E-05	-1,601836929	7,66E-06
RAP1GAP	-1,571112608	0,002977	1,168892538	0,220224
TFF1	-1,584119506	0,000215	1,026526455	0,767586
TSC22D1	-1,616857744	0,00075	-1,879048289	7,87E-05
RHOB	-1,707273726	2,64E-05	-4,267101563	7,97E-10
FHL1	-1,992656625	2,02E-05	-2,11291229	9,29E-06
CDH18	-2,044637464	0,000141	-1,944705571	0,000261
MT1F	-2,517448528	2,52E-05	-2,732116595	1,13E-05
cell cycle/proliferation inhibitors				
TSPAN13	-1,341011207	0,001989	-1,162470215	0,064723
FBXO4	-1,343238268	0,00044	-1,190087898	0,014609
E2F4	-1,348242117	0,000776	-1,189584577	0,022659
TP53INP1	-1,348390493	0,001801	-1,625258944	3,36E-05
HDAC1	-1,35523136	7,02E-05	-1,018092077	0,727663

RBL2	-1,411972962	0,001521	-1,368100279	0,002956
CREG1	-1,437544657	1,17E-05	-1,547601463	1,89E-06
RTKN	-1,455857165	0,019402	1,027848036	0,84597
PRKCD	-1,465776602	0,002264	-1,07726449	0,462124
MXD4	-1,469172735	0,007975	-1,077834212	0,544433
DUSP5	-1,492568657	0,027005	-1,050338727	0,761506
STC2	-1,514766507	0,000614	-1,122918866	0,217937
ADIPOR1	-1,591749322	6,85E-06	-1,336800406	0,000459
NR2F2	-1,620623423	2,15E-05	-2,297733652	8,82E-08
SOCS2	-1,63864273	0,007059	-2,367201364	0,000117
LRIG1	-1,970185246	2,49E-05	-1,437044657	0,006081
BTG1	-2,021573027	2,22E-05	-2,48332801	1,82E-06
EFEMP1	-2,504632082	3,96E-08	-2,744676259	1,42E-08
apoptosis				
LDOC1	-1,35901737	0,105565	-2,417070141	0,000326
TRIB3	-1,371297096	0,00303	-1,134207618	0,16238
PHLDA3	-1,390723569	0,000583	-1,608557746	2,50E-05
FASTK	-1,414327129	0,000663	-1,007112367	0,926319
TSC22D1	-1,414522749	9,57E-05	-1,781944147	7,04E-07
RPS27L	-1,452380564	1,72E-05	-1,752284775	2,92E-07
IFIT1	-1,456319273	0,023422	-1,568748289	0,009149
PPM1F	-1,461355694	0,001109	-1,099442341	0,302576
BCL2L13	-1,636184556	8,21E-06	-1,321207561	0,00113
BHLHE40	-1,636991122	4,07E-06	-1,033776998	0,591939
CERS6	-1,648999442	6,53E-06	-1,210013214	0,012203
STK25	-1,788496464	5,61E-08	-1,339253653	5,48E-05
DRAM1	-1,857101883	4,56E-05	-2,125307827	7,10E-06
SLC39A6	-2,334192998	2,31E-06	-2,321008519	2,47E-06
migration/invasion/angiogenesis inhibitors				
FOXA1	-1,356460032	0,001706	-1,034143346	0,662339
CITED4	-1,354405823	0,001696	-1,909148902	2,25E-06
EPHA4	-1,400971068	1,24E-06	-1,455333931	4,13E-07
CITED2	-1,657840051	8,46E-07	-1,637358522	1,09E-06
TNS3	-1,911609586	4,48E-07	-2,129502378	2,17E-06

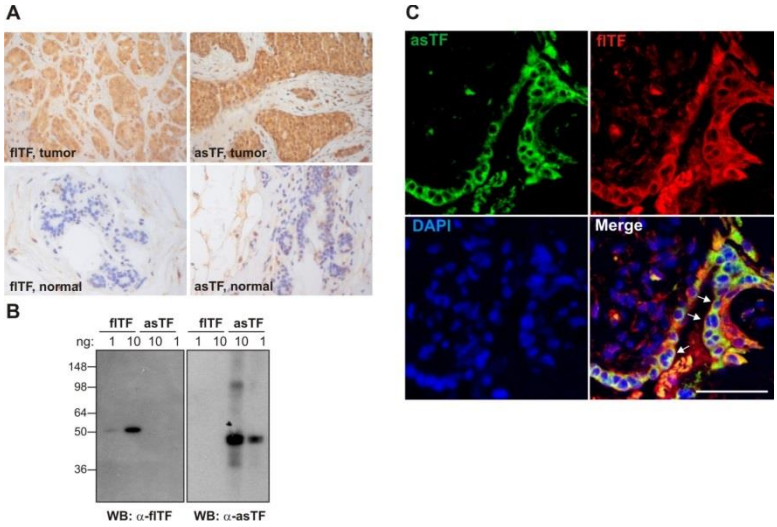

Fig. S1. asTF and flTF are overexpressed in human breast cancer specimens. (A) Representative photographs of tissue microarray punches of human breast cancer specimens (upper) and matched normal mammary tissue (lower) immunohistochemically stained using an flTF-specific (left) or an asTF-specific antibody (right). Brown color indicates positive staining. (Magnification: 20x). (B) Specificity of the anti-flTF and anti-asTF antibodies, tested on Western Blot. The indicated amounts of purified flTF and asTF proteins were loaded on gel. Note the asTF dimers migrating at 98 kDa. (C) Representative confocal image of a breast cancer specimen double-stained with the antibodies in (A). Note the intracellular staining of asTF (green) and the flTF staining at the cell periphery (red). Examples of peripheral staining are indicated by arrows. (Scalebar: 100 micron.)

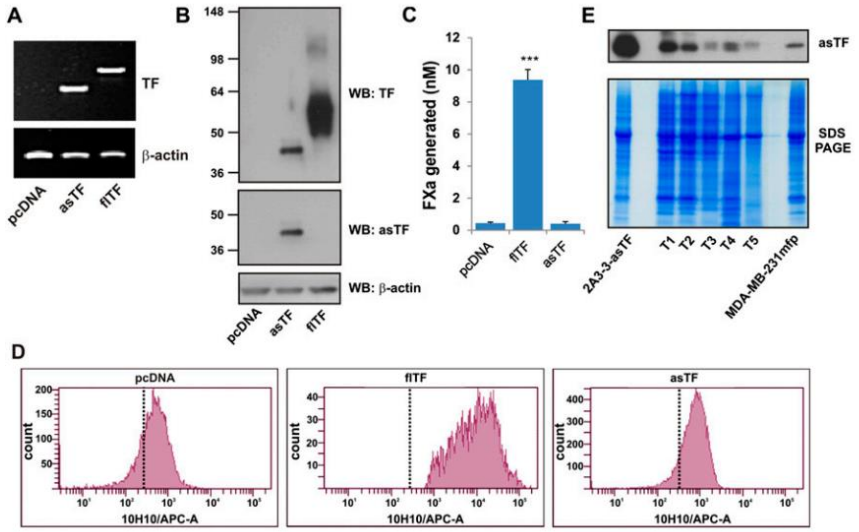

Fig. S2. Characterization of TF isoform-expressing 2A3-3 cells. (A) Control vector (pcDNA), flTF or asTF cDNA were stably integrated into the FRT site of 2A3-3 cells and TF isoform expression was verified by PCR using TF-specific primers. Primers against β-actin were used as a control. (B) Expression of flTF and asTF in 2A3-3 cells assessed by Western blot. Antibodies specific for total TF and asTF (monoclonal rabbit antibody RabMab1) were used. (C) TF activity of 2A3-3 control cells and cells expressing flTF or asTF was measured after addition of 10 nM FVIIa, and 100 nM FX in HBS. FXa generation was determined after 30 minutes using a Spectrozyme FXa kinetic assay. (D) FACS analysis of 2A3-3 control cells and cells expressing flTF or asTF. Cells were labeled in suspension with 1µg/ml 10H10 and APC-labeled rabbit anti-mouse secondary antibody. Labelled cells were analyzed on a Beckton Dickinson LSR II. Dashed lines indicate mean fluorescence intensity of the same cells, labeled with IgG control. (E) Protein (50µg) from lysates prepared from 2A3-3-asTF, MDA-MB-231-mfp cells and 5 tumor specimens with high asTF expression (as determined in the tissue array analysis) were subjected to Western blotting using anti-asTF RabMab1 as the primary antibody. The same samples were also loaded on SDS-PAGE and stained using Coomassie to verify equal loading. ***P<0.001

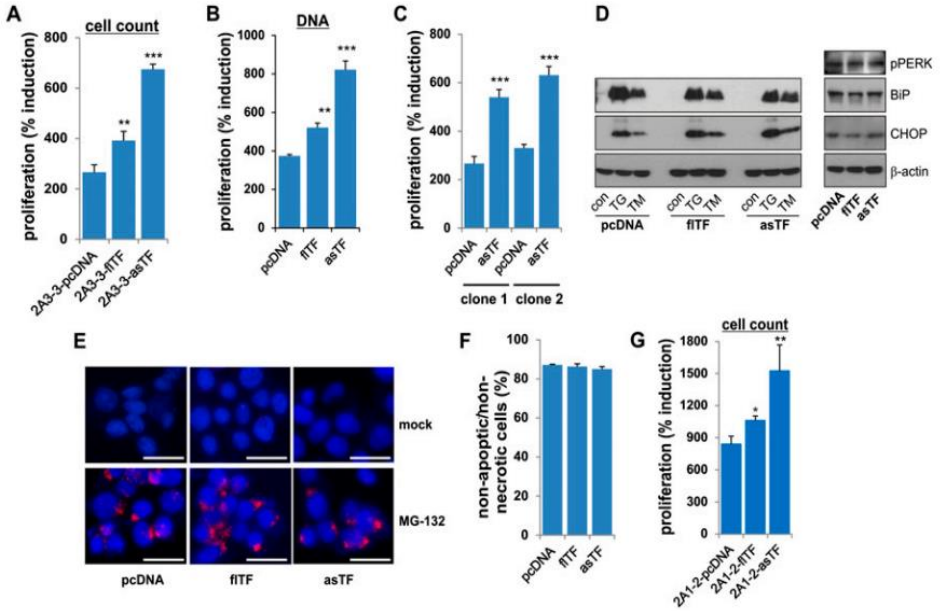

Fig. S3. Proliferation of asTF-expressing 2A3-3 cells. (A) Proliferation of 2A3-3 cells expressing TF variants was determined using cell counts. (B) Proliferation of 2A3-3 cells expressing TF variants was determined using DNA contents of cellular lysates at day 0 and day 3. Proliferation was expressed as % increase compared with day 0. (C) Enhanced proliferation of an independently generated second asTF clone was determined using MTT assays. (D) Activation of the unfolded protein response (UPR), as determined by Western blotting. The indicated cell lines were screened for up-regulation of UPR-responsive proteins CCAAT/enhancer/binding protein homologous protein (CHOP) and binding protein (BiP), and phosphorylation of protein kinase RNA-like endoplasmic reticulum kinase (PERK). β-actin was used as a loading control. (*Left*) A short exposure of CHOP and BiP levels in these cells, using established UPR activators [2 μM Thapsigargin (TG) and 10μg/ml Tunicamycin (TM)] as positive controls. (*Right*) basal levels (long exposure) of CHOP and BiP, and PERK phosphorylation in these cells. (E)Presence of cellular protein aggregates was determined using the ProteoStat protein aggregation kit (Enzo Life Sciences, Farmingdale, NY). The proteasome inhibitor MG-132 was used as an inducer of protein aggregation (positive control). Images were acquired with a conventional fluorescence microscope (Leica, DMI6000B). Scale bars: 20μM. (F)Apoptosis was assessed using annexin V-FITC staining and subsequent FACS analysis. (G) A cell line (2A1-2) containing an FRT site at a transcriptionally less active region was equipped with an empty vector, flTF or asTF cDNA by homologous recombination, and proliferation was monitored using cell counting.
*P<0.05, **P<0.01, ***P<0.001

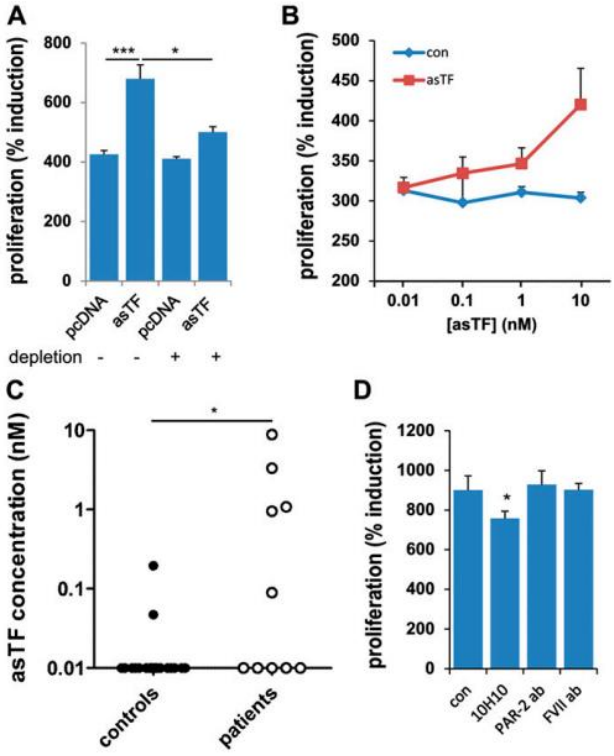

Fig. S4. Proliferation of 2A3-3-asTF cells is dependent on asTF secretion. (A) Conditioned medium of 2A3-3-asTF cells was left untreated or asTF-depleted using an asTF-specific antibody RabMab1. 2A3-3-pcDNA cells were cultured in these medium preparations, and proliferation was assessed 3 days later using MTT assay. (B) Effects of indicated amounts of recombinant asTF on 2A3-3-pcDNA cell proliferation using MTT. The experiment was controlled (con) by adding the identical corresponding amounts of the vehicle. (C) asTF concentrations were determined by plasma from 20 healthy control subjects and 10 metastatic breast cancer patients using an asTF-specific ELISA. (D) flTF cells were incubated with 50 µg/ml 10H10, PAR-2 blocking antibody or FVII-blocking antibody. Increases in cell numbers were determined on day 4, using MTT assay.
*P<0.05, ***P<0.001

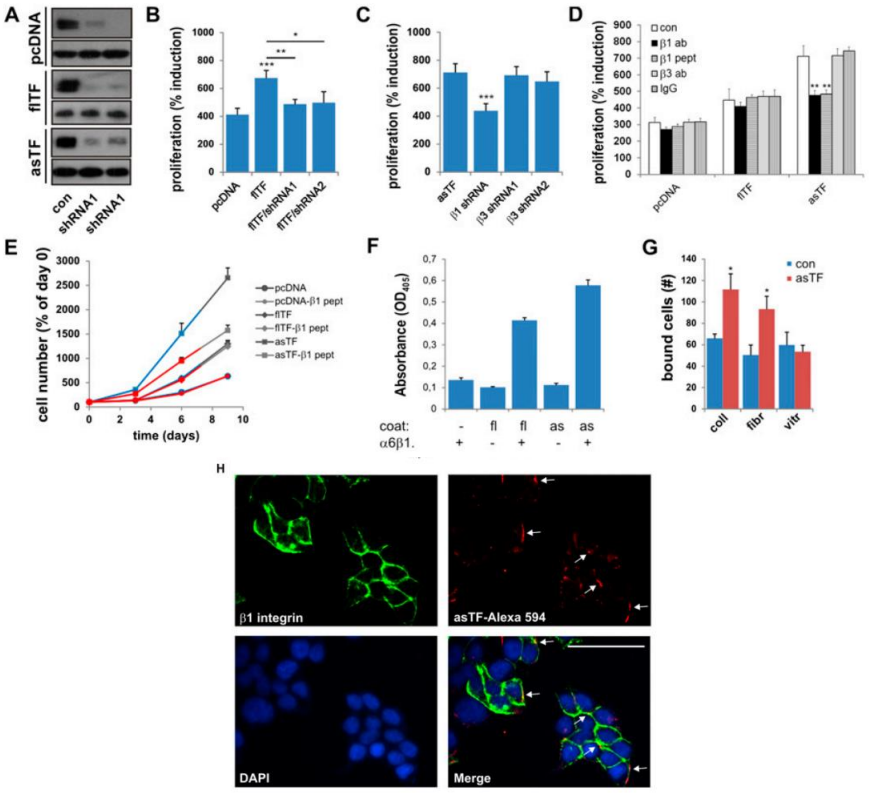

Fig. S5. Effect of integrin blockade on flTF-or asTF –expressing 2A3-3 proliferation. (A) 2A3-3-pcDNA, -flTF, and –asTF cells were transduced with β1 integrin shRNA lentiviral particles. The western blot shows β1 integrin expression levels after lentiviral transduction, β-actin is used as a loading control. (B) Proliferation of β1 silenced 2A3-3-flTF cells was assessed after 3 days using MTT and compared with that of control cells (pcDNA). (C) Cells were transduced with β1 integrin-specific shRNA particles or β3 integrin-specific shRNA particles as a control. Cell proliferation was determined by means of MTT assay. (D) 2A3-3 cells were incubated with antibodies against β1 integrins (residues 579-799) β3 integrins, or a peptide representing integrin β1 residues 579-799. (E) Proliferation was assessed after the days indicated as described. 2A3-3-pcDNA cells (circles), -flTF cells (diamonds), or -asTF cells (squares) were incubated with a β1 peptide resembling the β1 integrin region between residues 579-799 (1 nM). Proliferation was followed as in A. (F) The 96-wells plates were coated with asTF. Truncated flTF (sTF) coating was included as a positive control, as flTF was previously shown to bind to α6β1 integrins. Subsequently, the plates were incubated with the indicated recombinant integrin dimers, and bound integrin was detected using β1 antibody Ts2/16-HRP conjugated anti-mouse secondary antibody and colometric substrate (TMB). (G) 2A3-3-pcDNA cells were pre-incubated with 10nM recombinant asTF and seeded on collagen I, fibronection or vitronectin pre-coated dishes (all 10µg/ml) and left to adhere for 60 min. in Hepes-tyrode buffer. After washing, the remaining cells were counted.(H) pcDNA cells were grown on coverslips and incubated with 10 nM recombinant asTF conjugated to Alexa 594 for 20 minutes at ambient temperature. After fixation, cells were labeled with β1 antibody AIIB2 (green). Arrows indicate areas of extensive colocalization. Scale bar: 50 µm
*P<0.05, **P<0.01, ***P<0.001

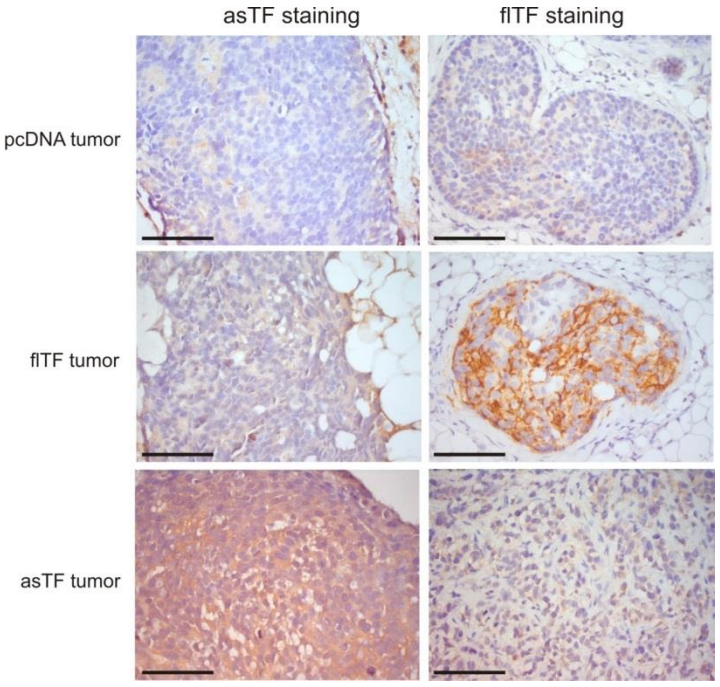

.

Fig. S6. Morphology and TF variant staining of 2A3-3 tumors. 2A3-3-pcDNA, -flTF or -asTF-derived tumors were extracted, fixed and stained using specific antibodies for asTF (left) or flTF (right). Sections were counterstained with hematoxylin. Note differences in flTF and asTF staining patterns and tumor morphology of pcDNA and flTF tumors versus asTF tumors. Scale bars represent:100 μm.

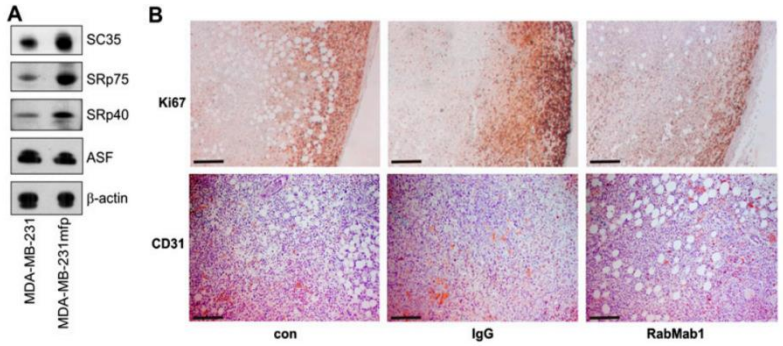

Fig. S7. Characterics of MDA-MB-231-mfp tumor cells and MDA-MB-231-mfp derived tumors. (A) Expression levels of SC35, SRp75, SRp40 and ASF/SF2 were determined on Western Blot. β-actin served as loading control (B)MDA-MB-231-mfp cells were co-injected with buffer control (con), 100 µg IgG control antibody or 100 µg RabMab1. Tumors were extracted, fixed in formalin, and stained for Ki67 (magnification:5x) or CD31 (magnification:10x). Notice the presence of mammary fat cells in the tumor specimens (white). Scale bars:200 µm.

gene	forward primer	reverse primer
LCP1	TGCCGGCAGTTTGTCACA	GGCAATAAAAGCCAAGTTCAACTT
FERMT2	AAAACAATGACCCCCACTTATGA	GTCACCAAACCAAGCAGAAGTTG
CCNA1	CCATCGACCTCAGCAAGCA	TGGCTCCATGAGGGACACA
MDK	GGTGCCCTGCAACTGGAA	ACGCACCCCAGTTCTCAAAC
FAM5c	CAGCACCCTTCGGAGACTTC	CCAGTCCGTGTTTCTGTTACCTT
MSLN	TGGACTTGGCCACGTTCAT	TGCACCTCAGCCACAGTCA
CDH18	AAACTTCACTCTGAAGGACAATGAAG	CCCATCTCTCTCGCATGCA
EFEMP1	CCAACCCTTCCCACCGTAT	TGTCTTGGCACACGTTGTGTT
DRAM1	AACTTGGTGTCTTTAGTGCTTGGA	ACTCCTGAAAATTGGCGACAA

Table S2. Primer pairs used in SYBR-Green based real-time PCR. Primer sequences are from 5’ to 3’. LCP1, lymphocyte cytosolic protein 1; FERMT2, fermitin family homolog 2; MDK, midkine; MSLN, mesothelin; CDH18, cadherin 18; EFEMP1, EGF containing fibulin-like extracellular matrix protein; DRAM1, DNA-damage regulated autophagy modulator 1; FAM5c, family with sequence similarity 5, member C.

Reference List

[1] Anczukow O, Rosenberg AZ, Akerman M, Das S, Zhan L, Karni R, et al. The splicing factor SRSF1 regulates apoptosis and proliferation to promote mammary epithelial cell transformation. Nat Struct Mol Biol 2012 Feb;19(2):220-8.

[2] Karni R, de SE, Lowe SW, Sinha R, Mu D, Krainer AR. The gene encoding the splicing factor SF2/ASF is a proto-oncogene. Nat Struct Mol Biol 2007 Mar;14(3):185-93.

[3] Venables JP, Klinck R, Bramard A, Inkel L, Dufresne-Martin G, Koh C, et al. Identification of alternative splicing markers for breast cancer. Cancer Res 2008 Nov 15;68(22):9525-31.

[4] Courtois S, Verhaegh G, North S, Luciani MG, Lassus P, Hibner U, et al. DeltaN-p53, a natural isoform of p53 lacking the first transactivation domain, counteracts growth suppression by wild-type p53. Oncogene 2002 Oct 3;21(44):6722-8.

[5] Datta D, Flaxenburg JA, Laxmanan S, Geehan C, Grimm M, Waaga-Gasser AM, et al. Ras-induced modulation of CXCL10 and its receptor splice variant CXCR3-B in MDA-MB-435 and MCF-7 cells: relevance for the development of human breast cancer. Cancer Res 2006 Oct 1;66(19):9509-18.

[6] Okumura N, Yoshida H, Kitagishi Y, Nishimura Y, Matsuda S. Alternative splicings on p53, BRCA1 and PTEN genes involved in breast cancer. Biochem Biophys Res Commun 2011 Sep 30;413(3):395-9.

[7] Radisky DC, Levy DD, Littlepage LE, Liu H, Nelson CM, Fata JE, et al. Rac1b and reactive oxygen species mediate MMP-3-induced EMT and genomic instability. Nature 2005 Jul 7;436(7047):123-7.

[8] Wang L, Duke L, Zhang PS, Arlinghaus RB, Symmans WF, Sahin A, et al. Alternative splicing disrupts a nuclear localization signal in spleen tyrosine kinase that is required for invasion suppression in breast cancer. Cancer Res 2003 Aug 1;63(15):4724-30.

[9] Van den Berg YW, Osanto S, Reitsma PH, Versteeg HH. The relationship between tissue factor and cancer progression: insights from bench and bedside. Blood 2012 Jan 26;119(4):924-32.

[10] Dorfleutner A, Hintermann E, Tarui T, Takada Y, Ruf W. Cross-talk of integrin alpha3beta1 and tissue factor in cell migration. Mol Biol Cell 2004 Oct;15(10):4416-25.

[11] Versteeg HH, Schaffner F, Kerver M, Petersen HH, Ahamed J, Felding-Habermann B, et al. Inhibition of tissue factor signaling suppresses tumor growth. Blood 2008 Jan 1;111(1):190-9.

[12] Bogdanov VY, Balasubramanian V, Hathcock J, Vele O, Lieb M, Nemerson Y. Alternatively spliced human tissue factor: a circulating, soluble, thrombogenic protein. Nat Med 2003 Apr;9(4):458-62.

[13] Bogdanov VY, Kirk RI, Miller C, Hathcock JJ, Vele S, Gazdoiu M, et al. Identification and characterization of murine alternatively spliced tissue factor. J Thromb Haemost 2006 Jan;4(1):158-67.

[14] Haas SL, Jesnowski R, Steiner M, Hummel F, Ringel J, Burstein C, et al. Expression of tissue factor in pancreatic adenocarcinoma is associated with activation of coagulation. World J Gastroenterol 2006 Aug 14;12(30):4843-9.

[15] Hobbs JE, Zakarija A, Cundiff DL, Doll JA, Hymen E, Cornwell M, et al. Alternatively spliced human tissue factor promotes tumor growth and angiogenesis in a pancreatic cancer tumor model. Thromb Res 2007;120 Suppl 2:S13-S21.

[16] Van den Berg YW, van den Hengel LG, Myers HR, Ayachi O, Jordanova E, Ruf W, et al. Alternatively spliced tissue factor induces angiogenesis through integrin ligation. Proc Natl Acad Sci U S A 2009 Nov 17;106(46):19497-502.

[17] Chandradas S, Deikus G, Tardos JG, Bogdanov VY. Antagonistic roles of four SR proteins in the biosynthesis of alternatively spliced tissue factor transcripts in monocytic cells. J Leukoc Biol 2010 Jan;87(1):147-52.

[18] Tardos JG, Eisenreich A, Deikus G, Bechhofer DH, Chandradas S, Zafar U, et al. SR proteins ASF/SF2 and SRp55 participate in tissue factor biosynthesis in human monocytic cells. J Thromb Haemost 2008 May;6(5):877-84.

[19] Contrino J, Hair G, Kreutzer DL, Rickles FR. In situ detection of tissue factor in vascular endothelial cells: correlation with the malignant phenotype of human breast disease. Nat Med 1996 Feb;2(2):209-15.

[20] Ryden L, Grabau D, Schaffner F, Jonsson PE, Ruf W, Belting M. Evidence for tissue factor phosphorylation and its correlation with protease-activated receptor expression and the prognosis of primary breast cancer. Int J Cancer 2010 May 15;126(10):2330-40.

[21] Srinivasan R, Ozhegov E, Van den Berg YW, Aronow BJ, Franco RS, Palascak MB, et al. Splice variants of tissue factor promote monocyte-endothelial interactions by triggering the expression of cell adhesion molecules via integrin-mediated signaling. J Thromb Haemost 2011 Oct;9(10):2087-96.

[22] Gentleman RC, Carey VJ, Bates DM, Bolstad B, Dettling M, Dudoit S, et al. Bioconductor: open software development for computational biology and bioinformatics. Genome Biol 2004;5(10):R80.

[23] Versteeg HH, Evertzen MW, van Deventer SJ, Peppelenbosch MP. The role of phosphatidylinositide-3-kinase in basal mitogen-activated protein kinase activity and cell survival. FEBS Lett 2000 Jan 7;465(1):69-73.

[24] van Nes JG, de Kruijf EM, Faratian D, van de Velde CJ, Putter H, Falconer C, et al. COX2 expression in prognosis and in prediction to endocrine therapy in early breast cancer patients. Breast Cancer Res Treat 2011 Feb;125(3):671-85.

[25] Bluff JE, Amarzguioui M, Slattery J, Reed MW, Brown NJ, Staton CA. Anti-tissue factor short hairpin RNA inhibits breast cancer growth in vivo. Breast Cancer Res Treat 2011 Aug;128(3):691-701.

[26] Wang HY, Lin W, Dyck JA, Yeakley JM, Songyang Z, Cantley LC, et al. SRPK2: a differentially expressed SR protein-specific kinase involved in mediating the interaction and localization of pre-mRNA splicing factors in mammalian cells. J Cell Biol 1998 Feb 23;140(4):737-50.

[27] Collier ME, Ettelaie C. Induction of endothelial cell proliferation by recombinant and microparticle-tissue factor involves beta1-integrin and extracellular signal regulated kinase activation. Arterioscler Thromb Vasc Biol 2010 Sep;30(9):1810-7.

[28] Jessani N, Humphrey M, McDonald WH, Niessen S, Masuda K, Gangadharan B, et al. Carcinoma and stromal enzyme activity profiles associated with breast tumor growth in vivo. Proc Natl Acad Sci U S A 2004 Sep 21;101(38):13756-61.

[29] Gupta V, Gylling A, Alonso JL, Sugimori T, Ianakiev P, Xiong JP, et al. The beta-tail domain (betaTD) regulates physiologic ligand binding to integrin CD11b/CD18. Blood 2007 Apr 15;109(8):3513-20.

[30] Xiong JP, Stehle T, Goodman SL, Arnaout MA. New insights into the structural basis of integrin activation. Blood 2003 Aug 15;102(4):1155-9.

[31] Luque A, Gomez M, Puzon W, Takada Y, Sanchez-Madrid F, Cabanas C. Activated conformations of very late activation integrins detected by a group of antibodies (HUTS) specific for a novel regulatory region (355-425) of the common beta 1 chain. J Biol Chem 1996 May 10;271(19):11067-75.

[32] Montanez E, Ussar S, Schifferer M, Bosl M, Zent R, Moser M, et al. Kindlin-2 controls bidirectional signaling of integrins. Genes Dev 2008 May 15;22(10):1325-30.

[33] Martuszewska D, Ljungberg B, Johansson M, Landberg G, Oslakovic C, Dahlback B, et al. Tensin3 is a negative regulator of cell migration and all four Tensin family members are downregulated in human kidney cancer. PLoS One 2009;4(2):e4350.

[34] Huang CS, Shen CY, Wang HW, Wu PE, Cheng CW. Increased expression of SRp40 affecting CD44 splicing is associated with the clinical outcome of lymph node metastasis in human breast cancer. Clin Chim Acta 2007 Sep;384(1-2):69-74.